-RESEARCH PAPER-

International Journal of Mining and Geo-Engineering

IJMGE

IJMGE 56-2 (2022) 125-138

DOI: 10.22059/IJMGE.2021.321666.594906

Constrained vertex optimization and simulation of the unconfined compressive strength of geotextile reinforced soil for flexible foundation construction

Daniel E. AJU [a], Kennedy C. Onyelowe [a, b, *]

[a] *Department of Civil Engineering, Michael Okpara University of Agriculture, Umudike, Nigeria*

[b] *Department of Civil and Mechanical Engineering, Kampala International University, Kampala, Uganda*

Article History:

Received: 08 April 2021.

Revised: 03 June 2021.

Accepted: 04 June 2021.

ABSTRACT

Extreme vertex design (EVD) provides an efficient approach to mixture experiment design whereby the factor level possesses multiple dependencies expressed through component constraints formulation. Consequently, the derived experimental points are within the center edges and vertices of the feasible constrained region. EVD was deployed for the modeling of the mechanical properties of the problematic clayey soil-geogrid blends. Geogrids are geosynthetic materials that possess an open mesh-like structure and are mostly used for soil stabilization. The geotextile materials present a geosynthetic and permeable layer to support the soil and foundation by improvement of its stiffness characteristics and at a cheaper cost to procure compared to other construction materials and possess unique lightweight properties with greater strength improvement on the soil layer when used. Minitab 18 and Design Expert statistical software was utilized for the mixture design experiment computation; to fully explore the constrained region of the simplex, I-optimal designs with a special cubic design model were utilized to formulate the mixture component ratios at ten experimental runs. I-optimality and D-optimality of 0.39093 and 1747.474, respectively, were obtained with a G-efficiency of 64.8%. The generated laboratory responses were taken together with the mixture ingredients' ratio and taken as the system database for the model development. Statistical influence and diagnostics tests carried out on the generated EVD model indicate a good correlation with the experimental results. Graphical and numerical optimizations were incorporated using a desirability function that ranged from 0 to 1, which helped to arrive at the optimal combination of the mixture components. 0.2% of geogrid, 9.8% of water, and 90 % of soil yielded the optimal solution with a response of 41.270kN/m2 and a desirability score of 1.0. The model simulation was further carried out to test the model's applicability with the results compared with the actual results using student's t-test and analysis of variance. The statistical results showed a p-value>0.05 which indicates a good correlation.

Keywords: *Geogrid; Unconfined compressive strength; Constrained simplex method; Design Expert*

1. Introduction

Construction of flexible road pavement with expansive subgrade soil most times requires higher thickness for constituting cross-section materials to safely carry the intending traffic loads without excessive and differential settlement of the subgrade [1]. Moreover, the flexible pavement could also deteriorate rapidly due to aggregated cross-section layers sinking into the expansive subgrade under traffic loads with increased moisture content. However, the introduction of a geosynthetic layer between the problematic clayey subgrade materials and the aggregate layer (base and sub-base) can prevent the dreadful intermixing of the soft subgrade with the sub-base and base layer which results in road failure [2]. The incorporation of geosynthetic materials can also provide significant gains in terms of thickness reduction of the pavement cross-section layers due to improved strength performance. Geogrid is a special type of geosynthetic material produced by stretching and extrusion of a high polymeric molecule (polyester, propylene, or high-density polyethylene (HDPE)). It possesses a number of apertures that are uniformly distributed between the transverse and longitudinal sections. Through the apertures, there is direct contact and bonding between the sheets of the geosynthetic materials and the soil particle [3-4].

Geosynthetics are non-natural materials often used to improve soil's mechanical properties. They are obtained from petro-chemical polymer-based plastics (polymeric materials) which are inert biologically and would not decompose due to the actions of fungal, bacteria, and microorganisms [5]. However, their chemical properties vary as most are totally inert while some are affected by sunlight and petrochemicals. They are incorporated with soil to achieve confinement, separation, and distribution of loads such as reinforcement for water pressure control and prevent soil movement while allowing water to pass through the material. It can also be effectively utilized to prevent or reduce base coarse aggregates horizontal deformation and to resist asphalt reflective cracking [6]. A pictorial illustration of the membrane tension effect of the geosynthetic materials when integrated as an ingredient in flexible road pavement construction is shown in Fig. 1 [7].

In line with the foregoing, utilization of geosynthetic materials in the construction of flexible road pavement has been a subject of rigorous research studies recently [7-8]; Wang et al. [9]; studied the creep behavior of geosynthetic-sand under varying loading levels in the construction and design of reinforced structures using a series of tests

* Corresponding author. *E-mail address:* kennedychibuzor@kiu.ac.ug (K. C. Onyelowe).

to derive the creep properties under varying loading levels through a self-developed experiment device. The obtained results indicate that under nonconstraint conditions, the creep rate of about 1.1 times contrary to the results obtained for the constraint condition. However, deformation due to creep was mainly observed at the endpoint pull-out of the geogrid, each strain zone measurement in terms of deformation is reduced to the fixed end of the geogrid from the tensile end.

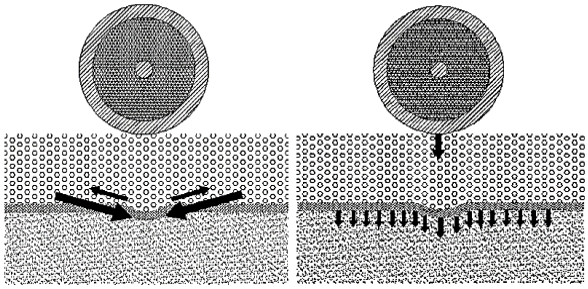

Fig. 1: Function of Geogrids in Flexible Road Pavement [7]

Furthermore, with the need to enhance the engineering properties of problematic subgrade soils using geosynthetic material to evaluate the relationships between the factor levels and their corresponding responses, advanced mixture design methods have been employed by several researchers [10-12]. Irving et al. [13]; research on the sphericity and roundness computation for particles using the extreme vertices model, the shape is a property studied for many kinds of particles. Among the shape parameters, sphericity and roundness indices have been largely studied to understand several processes. We have computed the relative difference respecting the model in the 512 × 512 × 512 space resolution. Note that the sphericity index is almost invariant in the worst tested case; the relative difference is less than 1%. Regarding the roundness index, in the worst tested case, the relative difference is less than 12%, this difference is bigger than that of the sphericity index due to EVM-roundness being highly dependent on the number of points. In addition, Faula Arina et al. [14] researched on Split Plot Mixture Process Variable Experiment on Steel Slag Concrete. The constraints of the mixture component affect the experimental region make it an irregular shape. XVERT algorithm was deployed to generate the required design points of the mixture experiment. A new split-plot design of mixture experiments with process variables was developed in this research with the investigation on the cementitious mixture components for steel slag concrete blend in five mixture components, namely; cement, aggregate fine, aggregate coarse, and percentage steel slag replacing aggregate fine and water. The process variable was the size of steel slag and the steel slag concrete experiment was run using a split-plot mixture process variable design with 23 whole plots of three observations.

The extreme vertex design (EVD) method is a mixture design technique, which occupies a sub-portion or smaller space within the simplex. The technique is essential when the design factor space selected is not L-simplex design. This limitation is imposed by both lower and upper bound constraints in the factor levels when there is a high level of interdependencies between the mixture components [15]. The major objective of the EVD method is to choose design points that appropriately cover the design space; this occurs as a result of additional constraints imposition of upper and lower boundary conditions on the mixture components which causes the design points to occupy some portion of the simplex known as the constrained region. The extreme vertex design technique permits the imposition of additional boundary limits on the mixture component values by specifying upper bounds on components and defining linear constraints for blends. The goal of using an extreme vertex design is to choose design points that adequately cover the design space [16].

For q-component mixtures where the i^{th} component proportion is present in the mixture by x_i, the factor space takes the shape of a regular (q-1) dimensional simplex due to the sum of one constraint presented in Eqn. 1. EVD method is flexible enough to deal with the imposition of additional constraints on the mixture components due to multiple dependencies between them. The lower and upper limit is denoted by L_i and U_i respectively. as shown in Eqn. 2 and the sum of the mixture component ratios must be unity [17].

$$\sum_{i=1}^{q} x_i = 1, \text{ i = 1, 2, 3... q } 0 \le x_i \le 1 \quad (1)$$

$$0 \le L_i \le x_i \le U_i \le 1 \quad (2)$$

The mixture experiments objective is to develop mathematical model adequate where the factor levels $(x_1, x_2, x_3, \ldots, x_q)$ relates the desired response parameters. Commonly used Scheffe's method for data fitting which is expressed in Eqn. 3 for quadratic polynomial function [18]

$$E(Y) = \sum_{i=1}^{q} \beta_i x_i + \sum \sum_{i<j}^{q} \beta_{ij} x_i x_j \quad (3)$$

and represented in matrix form as shown in Eqn. 4.

$$Y = X\beta + \varepsilon \quad (4)$$

Where X is $n \times k(\geq q)$ matrix and k is the number of model terms; Y is $n \times 1$ vector for the response parameter observations; ε is $n \times 1$ vector for the error function, and β is a $k \times 1$ vector for the predicted parameters [19-20].

The error properties were assumed to possess the property expressed in Eqn. 5

$$E(\varepsilon) = 0; E(\varepsilon\varepsilon') = \sigma^2 I_n \quad (5)$$

Where σ^2= the variance of the error function; I_n is an identity matrix.

The least-square estimator for the predicted variables β is presented in Eqn. 6.

$$b = (X'X)^{-1}X'Y \quad (6)$$

The variance-covariance matrix of the least-squares estimator solution (b) is further expressed in Eqn. 7.

$$Var(b) = (X'X)^{-1}\sigma^2 \quad (7)$$

This research study aims to investigate the utilization of geosynthetic materials for the improvement of the strength properties of weak subgrade soil. The problematic clayey soil-geogrid mixture experiment is carried out using the extreme vertex design method, which provides the flexibility to deal with multiple constraints associated with soil-geosynthetic combination to achieve improved durability and mechanical properties [20]. Moreover, the optimal mixture ingredients proportion is derived which produces the maximum mechanical strength response through desirability function using multiple criteria optimization which properly deals with the complex nature and multiple constraints of soil-geosynthetic blends. This research will contribute to existing knowledge on geosynthetic utilization for expansive soil stabilization for durable road pavement with better economic benefits [21].

2. Materials and Methods

2.1. Materials for Laboratory Methods

The experimental programs for the investigative study were carried out upon the guiding requirements stipulated in BS 1924 [22] and BS 1377 [23] for the problematic clayey soil mechanical properties improvement using geosynthetic materials. Classification and general engineering properties derivation of the test soil were first achieved through specific gravity test, consistency limit, compaction test, sieve analysis, and unconfined compressive strength (UCS) test. This mixture experiment problem, which involves three component materials, namely; geogrid, water, and clayey soil, and because of the component constraint imposition at the lower and upper boundary limits, the simplex is consequently constrained whereby the experimental points are situated at the vertices, interior and edges of the constrained region instead of the whole of the simplex [24]. Using I-optimal design computation with quadratic model design, the constrained experimental portion was adequately explored to generate the mixture components ratios and the number of experimental runs required. UCS tests were carried out with respect to the formulated ingredients proportions and the corresponding responses derived were utilized for the mechanical behavior modeling of the soil-geogrid blend. Statistical

influences and diagnostic tests were carried out to validate the developed EVD model. Furthermore, graphical and numerical optimization is conducted using desirability function computation to maximize the output variable criteria with respect to the factor levels. The optimal combinations of the soil-geogrid blend for maximum mechanical response were determined in this process followed by simulation of the EVD model [25-26]. The research program flowchart is presented in Fig. 2.

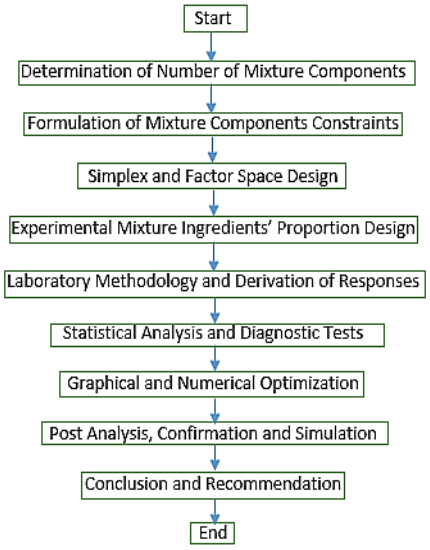

Fig. 2: Program Flowchart

2.1.1 Unconfined Compressive Strength

The unconfined compressive strength (UCS) is the maximum axial compressive stress that a right-cylindrical sample of material can withstand under unconfined conditions. The purpose of this laboratory is to determine the unconfined compressive strength of a cohesive soil sample. In this test, a cylinder of soil without lateral support is tested to failure in simple compression at a constant rate of the stream. The compressive load per unit area required to fail the specimen is called unconfirmed compressive strength of the soil in accordance with B.S.1377 (1975) [22] with a setup presented in Fig. 3.

Fig. 3: Unconfined compressive strength experimental setup

2.2. Test Materials

The materials and experimental steps that were undertaken towards achieving the objectives of this research were the focus. Expansive soil samples were collected at Edem Ekpenyong Street Anantigha, Calabar South Local Government Area of Cross River State, Nigeria. The geogrid (as presented in Fig. 4) was also obtained from Sermatech Construction Company in Calabar, Cross River State, Nigeria. Geogrids are spaced grid or open mesh-like synthetic materials constituting polymers cemented integrally as shown in Fig. 4. They have mechanical strength characteristics than common geosynthetic materials and can only stretch to a limit of about 2% - 5% under loading conditions [27-28]. The properties of the geogrid material used are shown in Table 3.

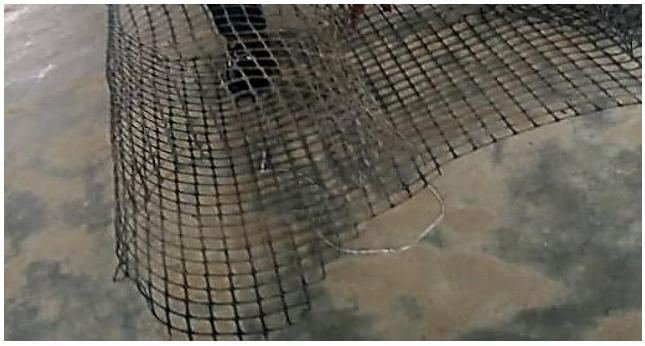

Fig. 4: Geogrid material

Table 1: Test Geogrid Properties

Descriptions	Units	Value
Aperture Size of Mesh	mm	10 x 10
Shape of Aperture	mm	Square
Tensile Strength	kN/m	12.5
Color		Black
Structure		Bi-directional
Elongation at maximum load	%	20.5
Unit Weight	N/m^3	7.35
Thickness of Sheet	mm	4
Raw Material		Polypropylene

2.3. Formulation of Geotextile Soil Specimen Mix Proportions

The determination of the actual proportion of the mixture ingredients to be mixed for each particular experimental run and the total number of experimental runs were carried out here. The effective ratios obtained here form the fundamental base for the EVD model development to derive the optimal combination ratio for the soil-geogrid blend and achieve improvement in the problematic clayey soil engineering properties for flexible pavement construction. The mixture formulation computation was carried out with Design Expert 11 and Minitab 18 statistical software [29-30].

2.3.1 Formulation of constraints

The mixture components are imposed with lower and upper bounds established through the properties of the ingredient materials which constitute the experimental soil-geogrid blend. In most cases, practical and environmental, economic, or physical considerations impose most of these boundary conditions. The three-component mixture investigated in this research study, constituting of geogrid, water, and problematic clayey soil to enhance its mechanical properties. From the relevant literature [31-33], the component constraints were formulated using single component constraints (SCC) are shown in Table 2.

2.3.2 Design of Simplex and Factor Space

The developed constraints, which defined the upper and lower limits of the single component constraints imposed on the factor levels, cause

the factor space to take a hyper-polyhedron simplex shape. The feasible experimental region within the simplex, termed the constrained space, is then obtained through the component constraints evaluation [34].

Table 2: Design Constraints

Mixture Coding:	Actual	
Low	Constraint	High
0.001	A:geogrid	0.002
0.098	B:water	0.150
0.848	C:soil	0.900
	A+B+C	1.000

The degree of freedom evaluation is also conducted through design matrix computation for the design mixture using a quadratic model with U_pseudo mixture component coding as presented in Table 3. A minimum of 3 lack of fit degrees of freedom (df) is required. This ensures a valid lack of fit test. Less df will result in a test that will not detect a lack of fit [29-30].

Table 3: Design Matrix Evaluation for Mixture Quadratic Model 3 Factors: A, B, C with U_Pseudo Mixture

Degrees of Freedom for Evaluation	
Model	5
Residuals	4
Lack of Fit	3
Pure Error	1
Corr Total	9

Power calculation test was also conducted on the developed component constraints using design expert and Minitab statistical software to determine the standard deviations and variances of the design planes, interior vertexes, and edges contained in the simplex on the 5% alpha level shown in Table 4.

Table 4: Power at 5 % alpha level to detect signal/noise ratio

Term	StdErr[1]	VIF	Ri-Squared	2 Std. Dev.
A	3376.29	33791.62	1.0000	5.0 %
B	0.90	2.99	0.6658	5.0 %
C	0.90	3.40	0.7063	5.0 %
AB	3468.84	13432.33	0.9999	5.0 %
AC	3468.52	16104.96	0.9999	5.0 %
BC	3.04	1.96	0.4908	51.6 %

^1 Basis Std. Dev. = 1.0

- Standard errors should be similar within the type of coefficients. Smaller is better.
- The ideal VIF value is 1.0. VIFs above 10 are a cause for concern. VIFs above 100 are a cause for alarm, indicating the coefficients are poorly estimated due to multi-co linearity.
- Ideal Ri-squared is 0.0. High Ri-squared means terms are correlated with each other, possibly leading to poor models.
- For mixture designs, the proportions of components must sum to one. This is a constraint on the system and causes multicollinearity to exist, thus increasing the VIFs and the Ri-squares, rendering these statistics useless; use a fraction of design space (FDS) instead.
- Power is inappropriate for determining the usefulness of a design involving mixture components. Use precision-based metrics provided in this program via FDS statistics [31-32].

The software further developed the contour plot of the 3- component simplex shown in Figs. 5-6, which diagrammatically displays the actual experimental points positioned within the constrained region. The information matrix measures showing the space type leverage, and build types are presented in Table 5. Ten (10) runs were generated to improve the optimality or efficiency of the model operation. Lack of fit was recorded on axialCB while the replicate point is situated at the center space of the feasible design space. The model build type was thus situated at the vertex and center-edge space type. Average leverage of 0.6 was calculated; this in effect raises concern for more design points to be located on these spaces of the simplex to reduce the lack of fit effect on the entire experimental space [35].

Table 5: Measures derived from the information matrix

Run	Leverage	Space Type	Build Type
1	0.8134	Vertex	Model
2	0.9129	Vertex	Model
3	0.5467	CentEdge	Model
4	0.8063	Vertex	Model
5	0.8335	Vertex	Model
6	0.3274	Center	Center
7	0.2710	AxialCB	Lack of Fit
8	0.5982	CentEdge	Model
9	0.5630	CentEdge	Model
10	0.3274	Center	Replicate
Average =	0.6000		

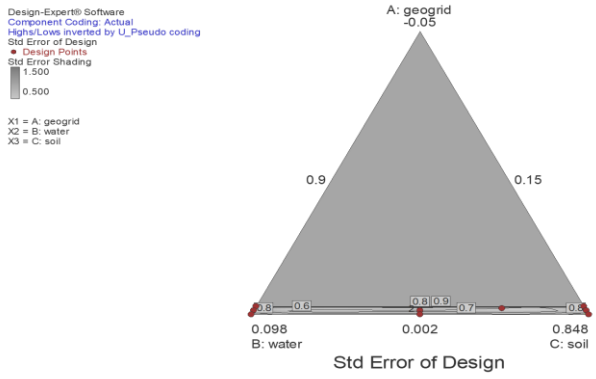

Fig. 5: Factor space simplex of a 3- component mixture experiment of water, soil, and geogrids.

The relevant data statistics for the design of experiments, multicollinearity design, scaled D-optimality, and I-optimal design computations were carried out using design expert software. D-optimality produces a design that best estimates the effects of the factors, which is particularly suited for screening studies. The algorithm picks points that minimize the volume of the confidence ellipsoid for the coefficients. I.e., it minimizes the determinant of the inverse matrix X'X, while I-optimal designs, also known as IV (integrated variance), provides a minimum average estimation of the variance across the experimental regions [36-37].

Condition Number of Coefficient Matrix = 2.16E+005

- If this value is 100-1000, there is moderate to strong multicollinearity.
- Values above 1000 indicate severe multicollinearity.

Maximum Variance Mean = 0.926

Average Variance Mean = 0.392

Minimum Variance Mean = 0.247

G Efficiency = 64.8 %

- G Efficiency is inversely related to the maximum variance.
- Lack of fit runs and replicates tend to reduce the G Efficiency of a design.

Scaled D-optimality Criterion = 1747.474

When comparing designs, a smaller value is better.

Determinant of (X'X)-1= 2.848E+13
Trace of (X'X)-1= 3.55E+007
I = 0.39093

- These can only be used when comparing designs with the same number of runs, a smaller value is better.

From the computation results, the design summary is thus presented in Table 6.

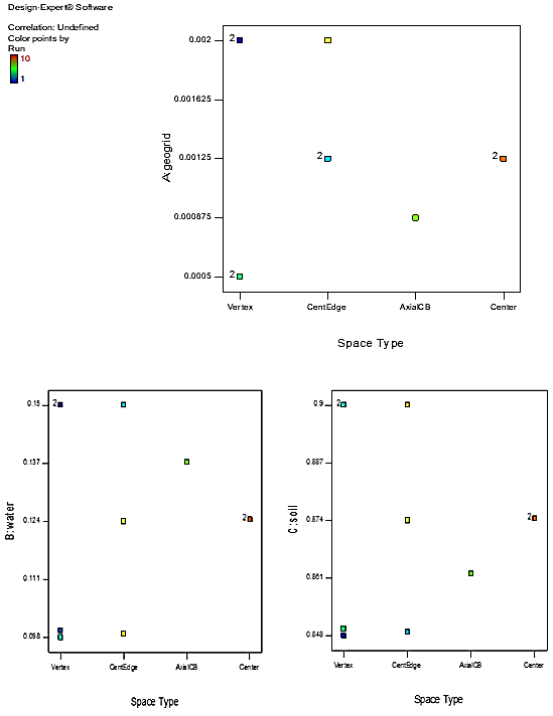

Fig. 6: Experimental factor space of the components in a 3- component mixture space

Table 6: Design Summary

File Version	10.0.0.3			
Study Type	Mixture		Subtype	Randomized
Design Type	I-optimal	Point Exchange	Runs	10
Design Model	Quadratic		Blocks	No Blocks

Component	Name	Units	Type	Minimum	Maximum	Mean	Std. Dev.
A	geogrid		Mixture	0.0005	0.002	0.0012875	0.000571456
B	water		Mixture	0.098	0.15	0.125619	0.0213172
C	soil		Mixture	0.848	0.9	0.873094	0.02129
				Total =	1.00	U Pseudo Coding	

2.3.3 Design of Experimental Mix Proportions

The number of experimental runs and the proportions of the ingredients were derived from the information matrix. Ten runs of experiments were derived in the process based on the imposed component constraints. Table 7 presents the mixes and runs for the 3-component multiconstraints experimental design. These mixes guide the preparation of specimens to be tested in the laboratory to achieve the responses [38-39].

3. Result Discussion and Analysis

3.1. Test Materials Characterization

The general classification and engineering behavior of the soil is presented in Table 8. The results indicate that it possesses high plasticity and swelling potential; it is also poorly graded and exhibits expansive properties of soft materials. The classification by AASHTO [40] and USCS [41] produced A-7 and CH, respectively, which indicates an unsuitable soil for engineering work with a low CBR of 5 %, MDD of 1.28 Mg/m3, and OMC of 17 %. The studied soil has a specific gravity of 2.38 and from the grain size distribution of the unaltered soil, 38.24 % were passed through BS No. 200 sieve (75 µm aperture). The plastic limit, liquid limit, and plasticity index results of 20.53%, 54.23%, and 33.7. According to the Federal Ministry of Works and Housing specification [42], the soils not suitable for subgrade materials possess liquid limit and plasticity index values =< 30% and =< 13% respectively which implies that samples fall outside the required specification. However, a stabilization process is required to improve its properties to make it suitable for civil works [43].

Table 7: Component experimental mix proportions for soil treatment with geogrids

	Component-1	Component-2	Component-3	Response	Pseudo- 1	Pseudo-2	Pseudo-3
Run	A:geogrid	B:water	C:soil	UCS	A:geogrid	B:water	C:soil
1	0.002	0.15	0.848		0.000	0.000	1.000
2	0.0005	0.0995	0.9		0.029	0.971	0.000
3	0.00125	0.15	0.84875		0.014	0.000	0.986
4	0.002	0.098	0.9		0.000	1.000	0.000
5	0.0005	0.15	0.8495		0.029	0.000	0.971
6	0.00125	0.124375	0.874375		0.014	0.493	0.493
7	0.000875	0.137187	0.861938		0.022	0.246	0.732
8	0.002	0.124	0.874		0.000	0.500	0.500
9	0.00125	0.09875	0.9		0.014	0.986	0.000
10	0.00125	0.1244	0.8743		0.014	0.493	0.492

Table 8: Basic properties of the test soil

Descriptions	Units	Value
Percentage Passing BS No. 200 Sieve (75 µm aperture)	%	38.24
Natural Moisture Content	%	36.45
Dry Unit Weight (γ_d)	kN/m³	17.69
Specific Gravity	-	2.38
Liquid Limit	%	54.23
Plastic Limit	%	20.53
Plasticity Index	%	33.7
OMC	%	17
MDD	g/cm³	1.28
AASHTO		A-7
USCS		CH
CBR	%	5
Unconfined Compressive Strength (UCS)	kN/m²	12.287

3.1.1 Particle Size Distribution Results

The sieve analysis result presents the size range of the particle present in the soil sample. According to the Federal Ministry of Work and Housing [42] specification requirement, for a sample to be used for road construction, the percentage of weight passing the No. 200 sieve shall be less than but not greater than 35%. The result shows 38.24% passing 0.075mm sieve size as shown in Table 9 and the plot in Fig. 7 which indicate highly plastic soil unsuitable for pavement subgrade materials. The gradation coefficients were then calculated using Eqns. 8 – 9.

Table 9: Sieve Analysis Results

Descriptions	Values										
Grain Size (mm)	4.75	3.18	2.4	1.2	0.6	0.42	0.3	0.21	0.15	0.075	0.053
Percent Finer (%)	99.32	98.63	97.6	73.55	69.2	67.2	65.25	60.22	52.15	38.24	2.5

Coefficient of Uniformity (C_u) = $\frac{D60}{D10}$ (8)

From the plotted semi-log graph: D_{60} = 0.21mm; D_{10} =0.073mm; D_{30} = 0.074mm

$C_u = \frac{0.21}{0.073} = 2.88$

Coefficient of curvature (C_c) = $\frac{(D30)^2}{D60 \times D10}$ (9)

$C_c = \frac{(0.074)^2}{0.21 \times 0.073} = 0.36$

Since $C_u < 4$ and $C_c < 1$, it showed that the soil sample according to the classification scale is a poorly graded fine silty clay sample [44].

3.2. Unconfined Compressive Strength (UCS) Test Results

The experimental parameters utilized for the Unconfined Compressive Strength (UCS) test of the soil-geogrid blend with a proven ring factor of 0.0009kN are presented below. The strain reading, corrected area, and stress values were then derived for each experimental run as shown in Table 10.

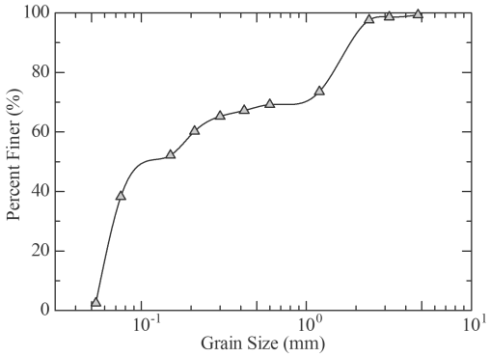

Fig. 7: Particle Size Distribution Graph

The soils were further blended with geogrid at varying ratios according to the mixture ratio formulated and the results computations carried out with the derived dimension and cross-sectional area of the mold are presented below [45-46];

Diameter of Mold = 5cm

Height of Mold (L) = 9.5cm

Proving Ring Factor = 0.0009kN

Area of mold (A) = $\frac{\pi d2}{4}$

A = $\frac{22x5x5}{7X4}$ = 19.64 cm^2

Volume of mold (V) = $\frac{\pi d^2 H}{4}$

V = $\frac{22x5x5x9.5}{7X4}$ = 186.61 cm^3

The major parameters' the formula utilized for this laboratory computation are presented in Eqns. 10-12, with the strain reading results and the actual length of the sample (L);

$$\text{Strain} \in (\%) = \frac{\Delta L}{L} \quad (10)$$

$$\text{Corrected Area } A_c = \frac{A_0}{1-\epsilon} \quad (11)$$

$$\text{Stress} = \frac{AxialForce}{CorrectedArea} \quad (12)$$

Table 10: UCS results summary

Experimental Runs	UCS Results Summary (kN/m²)
1	13.312
2	30.904
3	14.945
4	37.967
5	15.633
6	31.347
7	19.432
8	36.476
9	37.321
10	22.376

From the computed values, the maximum result of 37.97 kN/m^2 was obtained for the test (run 4) while the minimum of 13.312 kN/m^2 was obtained for the test (run 1) which indicates a significant improvement in the soil's compressive strength properties in line with the Federal Ministry of Works specification for subgrade materials. The result summary using percentage frequency statistics computation shows that 0.2% of geogrid, 9.8% of water, and 90% of soil by weight produced the maximum response of 37.97kN/m^2 for UCS target variable while 0.2% of geogrid, 15% of water, and 84.8% of soil by weight produced the minimum response of 13.312 kN/m^2 for UCS [47]. The stress-strain plot is presented in Fig. 8

4. Model Development and Validation

For the analysis after experimental reports were obtained, the appropriate transformation which is quadratic (square root) and the response ranges from 5.13527 to 18.9128 with a ratio of max to min of 3.683 for CBR response. Scheffe's models with intercepts built into the model coefficients are utilized for this mixture design. The transformation is required when the residual (error) is a function of the response magnitude (predicted results) and the transformation would be impactful unless the maximum to minimum ratio of the response parameter is very large [48-49].

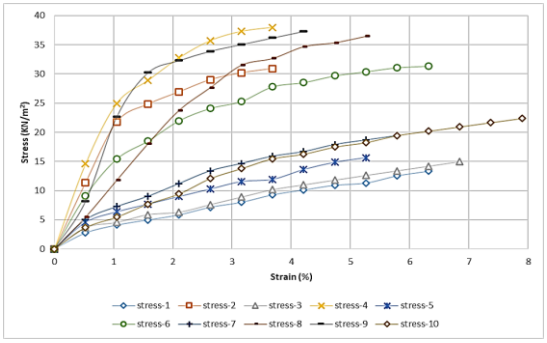

Fig. 8: UCS Stress vs. strain Plot

The fit summary, diagnostic tests, graphical and numerical optimization were carried out to determine the optimal combination proportion of the soil-geogrid blend to maximize the mechanical strength response. Post analysis, confirmation coefficient tables, and EVD model simulation were then executed to validate the model results using Design Expert 11 and Minitab 18 software [29-30].

4.1. Fit Summary

Fit summary brings together relevant statistics which were utilized for correction of the final model starting point through the Whitcomb score. The suggested models are selected and are considered a good starting point for model fitting. The fit summary presents the summary table with sequential and lack of fit P-value, the lack of fit tests, and model summary statistics which focuses on maximizing the adjusted and the Predicted R-squared [50]. The predicted residual error sum of squares (PRESS) is the measure of how much the model fits each of the experimental design points and is computed first of all by estimating where each point should be from a model which contains all points except the one under investigation shown in Eqn. 13.

$$PRESS = \sum_{i=1}^{n} (e - i)^2 \quad (13)$$

Where $e - i$ is the computed deletion residual by fitting a model without the ith run, then trying the estimate the ith observation of the model [31-32].

4.1.2 Fit Summary for UCS Response

The model fit summary statistics results is shown in Tables 11-13 indicated a preference for a quadratic model for CBR response with R-squared, predicted, adjusted and R-squared of 0.8367, 0.6417, and 0.79 respectively. The lack of fit test results presented a sum of squares of 1.09, a mean square of 0.18, and a lack of fit p-value (Prob > F) of 0.8010.

4.2. Analysis of Variance (ANOVA) Test Result

ANOVA statistics were carried out by using the linear model which was prescribed for the target variables to determine the statistical significance of the mixture factor levels using pseudo coding with respect to UCS response parameters [51]. The partial sum of squares result is presented for the corresponding model coefficients using p-values (Prob > F) for statistical significant determination criteria, which is computed using the mean square and F-value as shown in Tables 14-15.

Table 11: Model Summary Statistics for UCS response

Source	Std.Dev.	R-Squared	Adjusted R-Squared	Predicted R-Squared	PRESS	
Linear	0.46	0.8367	0.7900	0.6417	3.21	Suggested
Quadratic	0.45	0.9105	0.7987	0.4003	5.37	
Special Cubic	0.37	0.9548	0.8643	0.8129	1.68	
Cubic	0.61	0.9579	0.6211		+	Aliased

+ Case(s) with leverage of 1.0000: PRESS statistics was not defined

Table 12: Lack of Fit Test for UCS response

Source	Sum of Squares	df	Mean Square	F Value	p-value Prob > F	
Linear	1.09	6	0.18	0.48	0.8010	Suggested
Quadratic	0.42	3	0.14	0.38	0.7990	
Special Cubic	0.028	2	0.014	0.037	0.9646	
Cubic	0.000	0				Aliased
Pure Error	0.38	1	0.38			

"Lack of Fit Tests": Want the selected model to have insignificant lack-of-fit.

Table 13: Sequential Model Sum of Squares [Type I] for UCS response

Source	Sum of Squares	df	Mean Square	F Value	p-value Prob > F	
Mean vs Total	250.75	1	250.75			
Linear vs Mean	7.50	2	3.75	17.93	0.0018	Suggested
Quadratic vs Linear	0.66	3	0.22	1.10	0.4459	
Sp Cubic vs Quadratic	0.40	1	0.40	2.93	0.1854	
Cubic vs Sp Cubic	0.028	2	0.014	0.037	0.9646	Aliased
Residual	0.38	1	0.38			
Total	259.71	10	25.97			

4.2.1 R-squared Calculation

R-squared is the measure of the variation around the mean explained by the model in Eqn. 13

$$R^2 = 1 - \left[\frac{SS_{residual}}{SS_{residual} - SS_{model}}\right] \quad (13)$$

R-squared is a measure of the variation around the model explained mean, which is adjusted for the model number of terms. The adjusted R-squared decreases as the model number of terms increases, which do not add an additional value to the model results. Predicted R-square is the measure of the variation in the new result explained by the model, the difference between the predicted R-square and R-square will be less than or equal to 0.2, else this will result in the data fitting problem. However, factor transformation or outliers would be carried out to remedy the situation [52].

Table 14: ANOVA Results for UCS response

Response	2	UCS	
Transform:	Square Root	Constant:	0

ANOVA for Quadratic Mixture model
***** Mixture Component Coding is U_Pseudo. *****
Analysis of variance table [Partial sum of squares - Type III]

Source	Sum of Squares	df	Mean Square	F Value	p-value Prob > F	
Model	8.16	5	1.63	8.14	0.0319	significant
^Linear Mixture	7.50	2	3.75	18.71	0.0093	
AB	0.037	1	0.037	0.18	0.6913	
AC	0.034	1	0.034	0.17	0.7033	
BC	0.48	1	0.48	2.39	0.1970	
Residual	0.80	4	0.20			
Lack of Fit	0.42	3	0.14	0.38	0.7990	not significant
Pure Error	0.38	1	0.38			
Cor Total	8.96	9				

^1 inference for linear mixtures uses Type I sums of squares.

- The Model F-value of 8.14 implies the model is significant. There is only a 3.19% chance that an F-value this large could occur due to noise.
- Values of "Prob > F" less than 0.0500 indicate the model terms are significant. In this case, B, C is significant model terms. Values greater than 0.1000 indicate the model terms are not significant.
- If there are many insignificant model terms (not counting those required to support hierarchy), model reduction may improve your model.
- The "Lack of Fit F-value" of 0.38 implies the lack of Fit is not significant relative to the pure error. There is a 79.90% chance that a "Lack of Fit F-value" this large could occur due to noise. Non-significant lack of fit is good -- we want the model to fit [31-32].

Tables 15: R-squared Calculations for UCS response

Std. Dev.	0.45	R-Squared	0.9105
Mean	5.01	Adj R-Squared	0.7987
C.V. %	8.94	Pred R-Squared	0.4003
PRESS	5.37	Adeq Precision	7.791
-2 Log Likelihood	3.14	BIC	14.65
		AICc	28.14

The "Pred R-Squared" of 0.4003 is not as close to the "Adj R-Squared" of 0.7987 as one might normally expect; i.e. the difference is more than 0.2. This may indicate a large block effect or a possible problem with your model and/or data. Things to consider are model reduction, response transformation, outliers, etc. All empirical models should be tested by doing confirmation runs. "Adeq Precision" measures the signal-to-noise ratio. A ratio greater than 4 is desirable. Your ratio of 7.791 indicates an adequate signal. This model can be used to navigate the design space (Akhnazarova et al. 1982) [53].

4.3. Coefficient estimates and model equations for UCS

The estimates of components' coefficient, standard error, degrees of freedom, variance inflation factor (VIF), and final equation in terms of L_pseudo component computation results are presented in Tables 16-18. VIF measures the extent to which the variance of the coefficient estimate (predictor) is inflated by a lack of orthogonality in the design points. If the factor is orthogonal with respect to all other factors in the model, then VIF = 1 [54].

Table 16: Model Coefficients Calculation Results for UCS response

Component	Coefficient Estimate	df	Standard Error	95% CI Low	95% CI High	VIF
A-geogrid	621.93	1	1511.45	-3574.53	4818.40	33791.62
B-water	6.41	1	0.40	5.29	7.52	2.99
C-soil	3.82	1	0.40	2.70	4.95	3.40
AB	-663.30	1	1552.89	-4974.80	3648.21	13432.33
AC	-635.46	1	1552.74	-4946.56	3675.64	16104.96
BC	2.10	1	1.36	-1.67	5.88	1.96

Table 17: Final Equation in Terms of U_Pseudo Components

	*A	*B	*C	*AB	*AC	*BC
Sqrt(UCS) =	621.935	64.085	11.82484	-663.296	6315.46	3.10192

The equation in terms of coded factors can be used to make predictions about the response for given levels of each factor. By default, the high levels of the factors are coded as +1 and the low levels of the factors are coded as -1. The coded equation is useful for identifying the relative impact of the factors by comparing the factor coefficients [29-30].

Table 18: Final Equation in Terms of U_Pseudo Components

	*Geogrid	*Water	*Soils	Geogrid* Water	Geogrid* Soil	Water*Soil
Sqrt(UCS) =	2.36E+05	-615.29836	-3.1977	-2.45E+05	-2.35E+05	777.336

The equation in terms of actual factors can be used to make predictions about the response for given levels of each factor. Here, the

levels should be specified in the original units for each factor. This equation should not be used to determine the relative impact of each factor because the coefficients are scaled to accommodate the units of each factor and the intercept is not at the center of the design space [18].

4.4. Diagnostics Plots

The model statistical diagnostics computations were deployed for the verification of regression model assumptions depending on observations with undue or substantial influence on the statistical analysis using the studentized residual which is the quotient of the residual and its predicted standard deviation. Externally Studentized residuals are the default with Internally Studentized and raw residuals as options. Unless the leverages of all runs in a design are identical, the standard errors of the residuals are different. This means that each raw residual belongs to different populations (one for each different standard error). Therefore, raw residuals should not be used for checking the regression assumptions. Studentizing the residuals maps all different normal distributions to a single standard normal distribution. Externally Studentized residuals based on a deletion method are the default due to being more sensitive for finding problems with the analysis. Internally Studentized residuals are also available but are less sensitive to finding such problems [55-56].

4.4.1. Normal probability plot

The normal probability plot certifies that the error functions are normally roughly distributed, which implies that the residuals are positioned near the line of fit and not far away. It has essential significance for the model prediction performance. Definite shape patterns are searched for like an "S-shaped" curve, which indicates that a response transformation may provide a better analysis [57]. Normal probability plots for UCS responses are presented in Fig. 9

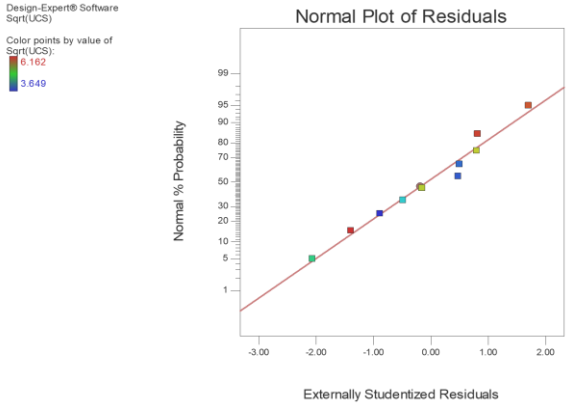

Fig. 9: Normal Plot of Residuals for UCS response

4.4.2 Residual vs. predicted plot

This statistical diagnostic test verifies the constant variance assumption using externally studentized residuals on the y-axis and the predicted values on the x-axis as shown in Fig. 10. The result implies the need for a transformation due to the observed expanding variance. The scattered plot was very close to the zero studentized residual points with the minimum and maximum of -7.45332 and 7.45332 for UCS target response [58].

4.4.3 Residuals vs. Run

This is a plot of the residuals or error versus the experimental run order. It checks for lurking variables that may have influenced the output response during the experiment as shown in Fig. 11. The plotted result should show a randomly scattered path and the studentized residuals with respect to the experimental runs are close to the line. Trends indicate a time-related variable lurking in the background. Blocking and randomization provide insurance against trends ruining the analysis (Schwartz et al. 1981) [59].

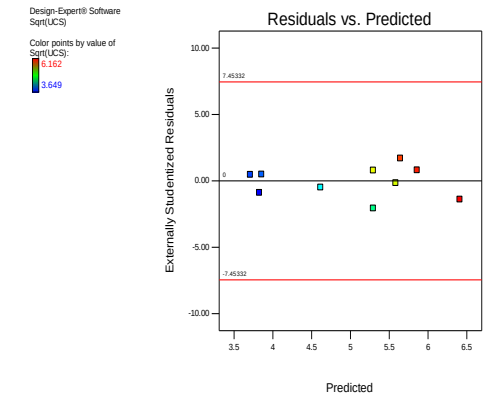

Fig. 10: Residuals vs. Predicted for UCS response

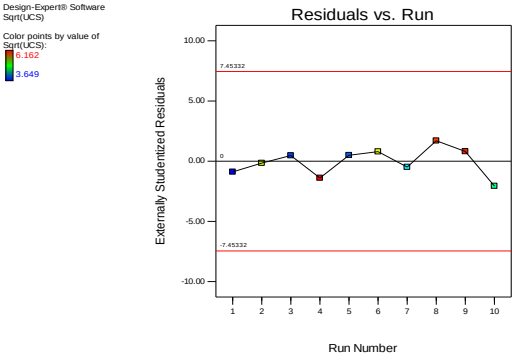

Fig. 11: Residuals vs. Run for UCS Response

4.4.4 Predicted vs. Actual

This diagnostic plot shows the predicted EVD model response values on the y-axis against the actual values on the x-axis. This plot could also help to determine the value or a group of values that are not estimated easily by the EVD model in terms of accuracy as presented in Fig. 12. The result deduced from the plotted results indicates a strong correlation between the experimental and the model predicted values with the plotted datasets ranging from about 3.5-6.5 [60].

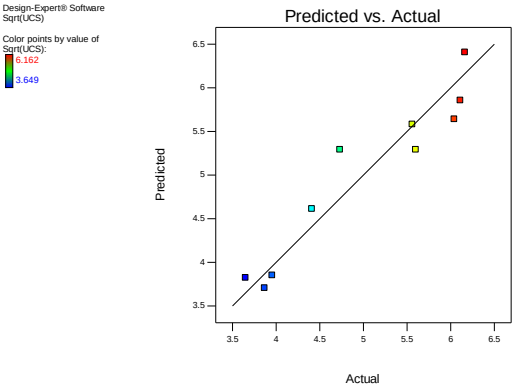

Fig. 12: Predicted vs. Actual UCS response

4.4.5 Box-Cox plot for power transforms

This diagnostic plot test provides guidelines for power-law transformation selection. Based on the derived best value for lambda, a recommended transformation is then listed which is situated at the lowest point of the curve generated by the natural log of the sum of squares of the residuals as presented in Fig. 13. The result presents the best point of 5.02197 for the sum of the residuals of squares which showed the best and current lambda, at -1.53 and 0.5 respectively at low and high confidence intervals (C.I.) of -4.15 and 2.66 respectively [61].

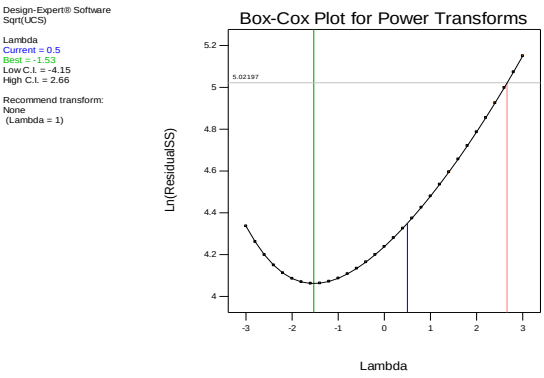

Fig. 13: Box-Cox Plot for Power Transformation

4.5. Influence Plots

These computational results provide measures of the influence, potential or actual, of individual runs. The graphical plots provide a clearer perspective on whether a case or two stick out from the others group sets. The statistical influences were assessed through cook's distance, leverage vs. the experimental run, and DFFITS statistics vs. experimental run [62].

4.5.1 Cook's distance

The Cook's distance is utilized for the determination of the statistical data points influenced in an ordinary least squares regression analysis problem. The influential points are worth particularly for validity confirmation and to present planes of the feasible experimental design space where better performance can be achieved. A measure of how much the entire regression function changes when the i^{th} point is used is not included in fitting the model. It is essentially the sum of differences in predictions at every point caused by leaving a point out for fitting the model [63]. The Cook's distance plots for the UCS responses are shown in Fig. 14. The presented result indicates that the Cook distance scores are mostly within the 0 - 1 limit while experimental run no. 4 were observed to fall outside the limit to be positioned between 1.2 and 1.0.

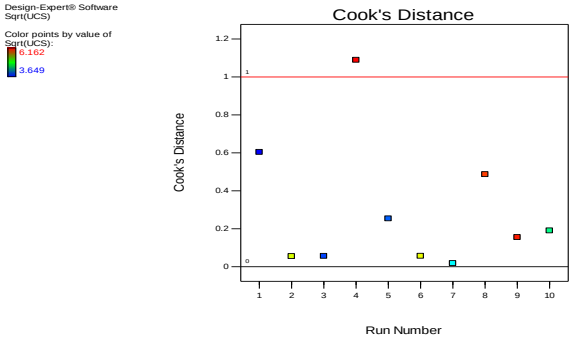

Fig. 14: Cook's distance for UCS response

4.5.2 Leverage vs. Run

Leverage evaluates how much each of the experimental points influences the fitness of the model. If the experimental point produces a leverage of 1.0, then the model performance exactly fits the observation at that point which controls the model output. A run with leverage greater than 2 times the average is generally regarded as having high leverage. Such runs have few other runs near them in the factor space as shown in Fig. 15. The plotted results indicated a straight leverage line at 0.6 which divided the scattered plot of the results into two [64].

4.5.3 DFFITS vs. Runs

DFFITS is a diagnostics statistical technique that shows the behavior of the influential experimental points in a regression analysis computation. A measure of how much the prediction changes at the i^{th} point when the i^{th} point is not included for fitting the model as shown in Fig. 16.

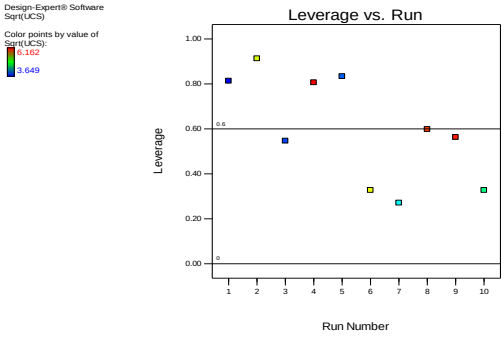

Fig. 15: Leverage vs. Run

The plotted results indicate DFFITS points with respect to the experimental runs lie very close to the zero points within the regions of ±2.32379 for the output responses. Experimental run no. 4 was also observed to be positioned outside the boundaries at about DFFITS of about -3 [65].

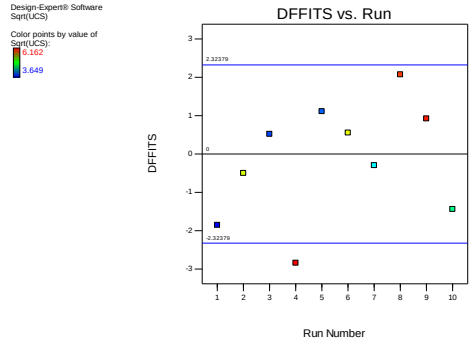

Fig. 16: DFFITS vs. Run for UCS Response

4.5.4 Diagnostic Plots and Influence Statistics Summary Report

The statistical diagnostic plots and influence summary report present the predicted and actual values, lambda values, leverage, internally and externally studentized residuals with respect to the generated standard order for the two response cases as shown in Table 19. The box-cox power transformation computation results show the best lambda values of -1.53, 95% CI Low and high values of -4.15 and 1.53, respectively, for the UCS response [29-30].

Box-Cox Power Transformation				
Constant k	95% CI Low	95% CI High	Best Lambda	Rec. Transform
0.000	-4.15	2.66	-1.53	None

4.6. Numerical Optimization Computation

In addition to the model validation in terms of numerical application of the solution variability, an overall desirability function (D) is incorporated and utilized as a metric for multicriteria optimization. For each criterion fixed values ranging from 0 and 1 are defined such that the desirability function scale satisfies the following conditions $0 \leq d(y_i) \leq 1$. If 0 is obtained, it implies that one or more criteria are situated outside their acceptable limit values; then if 1 is obtained; it signifies that the obtained solutions lay exactly at the acceptable response limits and the acceptability or rejection conditions depend generally on the objective function which is defined as the optimization direction through the minimization and maximization of the target through the reference equations [66].

Where the minimized response indicates that a minimum or lesser value is desired and thus the desirability function is represented in Eqn. 14.

Table 19: Summary Report on the Influence and Diagnostic Plots for

Response	UCS				Transform:	Square Root	Constant:	0.000	
					Diagnostics Case Statistics				
Run Order	Actual Value	Predicted Value	Residual	Leverage	Internally Studentized Residual	Externally Studentized Residual	Cook's Distance	Influence on Fitted Value DFFITS	Standard Order
1	3.65	3.82	-0.18	0.813	-0.912	-0.887	0.604	-1.852	10
3	3.87	3.71	0.16	0.547	0.528	0.474	0.056	0.521	9
5	3.95	3.85	0.10	0.833	0.551	0.497	0.254	1.111	8
7	4.41	4.61	-0.21	0.271	-0.539	-0.485	0.018	-0.296	7
8	6.04	5.64	0.40	0.598	1.400	1.699	0.487	2.073	6
10	4.73	5.29	-0.56	0.327	-1.532	-2.063	0.190	-1.439	5
6	5.60	5.29	0.31	0.327	0.834	0.795	0.056	0.555	4
4	6.16	6.41	-0.25	0.806	-1.253	-1.392	1.089[1]	-2.840[1]	3
9	6.11	5.86	0.25	0.563	0.850	0.813	0.155	0.923	2
2	5.56	5.58	-0.023	0.913	-0.177	-0.154	0.055	-0.499	1

[1] Exceeds limits.

$$d(y_i) = \begin{Bmatrix} 0 & y_i < T \\ \left(\frac{U - y_i}{U - T}\right)^{r_i} & T \le y_i \le U \\ 0 & y_i > U \end{Bmatrix} \quad (14)$$

For the second condition, a maximized response indicates that a larger value is derived and thus the desirability functions are represented in Eqn. 15.

$$d(y_i) = \begin{Bmatrix} 0 & y_i < L \\ \left(\frac{y - L}{T - L}\right)^{r_i} & L \le y_i \le T \\ 1 & y_i > T \end{Bmatrix} \quad (15)$$

Finally, for this condition, the target response which indicates the best value (response) and the desirability function for this case is presented in Eqn. 16.

$$d(y_i) = \begin{Bmatrix} 0 & y_i < L \\ 0 & y_i < U \\ \left(\frac{U - y_i}{U - T}\right)^{r_i} & T \le y_i \le U \\ \left(\frac{y - L}{T - L}\right)^{r_i} & L \le y_i \le T \end{Bmatrix} \quad (16)$$

Where; T is the target or actual (experimental) value, y_i is the model predicted value of the ith response, L is the lower limit or lowest acceptable results or values, r_i is the weighted function of the ith desirability function and U is the maximum or highest acceptable results or values. Based on the given conditions presented in the equations above, a multi-response numerical optimization is executed through which the optimum mix combination is maximized through the weighted geometric mean of individual desirability function $d(y_i)$ from the feasible composite space [67]. Through this optimization process, a model with equal weight is then adopted through the composite desirability by using the mathematical equation of the form, where n is the total individual number of responses in Eqn. 17.

$$D = [d(y_1) \times d(y_2) \times d(y_3) \ldots \times d(y_n)]^{1/n} \quad (17)$$

4.6.1 Optimization Overview

Numerical optimization uses the model to search the factor space for the best trade-offs to achieve multiple goals. The optimization module searches for a combination of factor levels that simultaneously satisfy the criteria placed on each of the responses and factors. The goals that apply to both responses and factors were set to be in the range for the factors and maximize for the response where the lower limit is the lowest acceptable outcome and the upper limit is the desired best result as shown in Table.

The mixture optimization solution is presented in Table 21. In the desirability function computation, the solution with the highest score is preferentially taken as the optimal solution.

Table 20: Optimization Criteria Definition

Name	Goal	Lower Limit	Upper Limit	Lower Weight	Upper Weight	Importance
A:geogrid	is in range	0.0005	0.002	1	1	3
B:water	is in range	0.098	0.15	1	1	3
C:soil	is in range	0.848	0.9	1	1	3
UCS	maximize	13.3119	37.9672	1	1	3

A desirability criterium score of 1.0 and optimal ratio 0.002:0.098:0.9 for the fraction of geogrid, water, and soil, respectively [29-30].

Table 21: Optimization Solutions

Number	geogrid	water	soil	CBR	Desirability	
1	0.002	0.098	0.900	19.546	1.000	Selected
2	0.002	0.105	0.893	19.112	1.000	
3	0.002	0.103	0.895	19.244	1.000	
4	0.002	0.100	0.898	19.429	1.000	
5	0.002	0.107	0.891	18.933	1.000	
6	0.002	0.099	0.899	19.480	1.000	
7	0.002	0.106	0.892	19.005	1.000	
8	0.001	0.118	0.881	6.039	0.207	

4.6.2 Optimization Ramps and Bar Graph

The numerical optimization ramps show the optimal solution graphical view with the optimal predictor parameter factor settings in red and the optimal response parameter factor in blue. This tool helps to make the required selection of the optimal solution in a graphical view presentation as shown in Fig. 17. Desirability value of 1.0 was calculated for the mixture component variables and the response variables, which indicate a robust model prediction of the mechanical behavior of soil-geogrid blend [35-37].

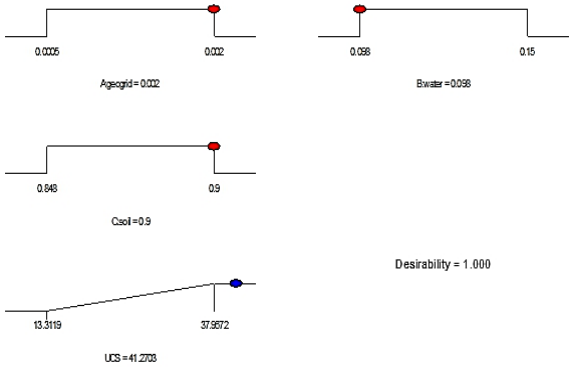

Fig. 17: Optimization Ramps

4.6.3 Optimization Trace Plot

Trace plots as presented in Fig. 18 are used to assess all mixture components effects in the factor space and its essence is to determine the response function sensitivity compared to the deviation from the formulation of the reference blend in U_pseudo coding. The results indicate that mixture component 'B' which is geogrid produces the dominant effect in the mixture due to the low mass ratio of component 'A' (geogrid) with the high/low limit values inverted by U_pseudo coding [68].

4.6.4 Optimization Contour Plot

A contour plot is an important tool for the visualization of the feasible experimental region's functional points in the iteration solution of mixture optimization [69]. The contour plot for the optimal solution for the design points for UCS are ranging from 13.3119 to 37.9672 and the desirability points from 0 to 1. It is a graphical tool for the representation of 3-D surfaces by contour plotting in terms of constant slices in 2-D form as shown in Fig. 19.

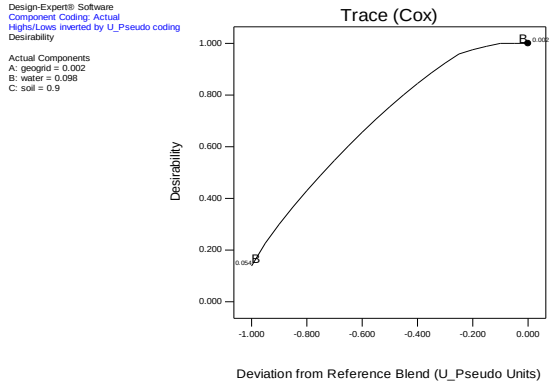

Fig. 18: Trace Cox Plot

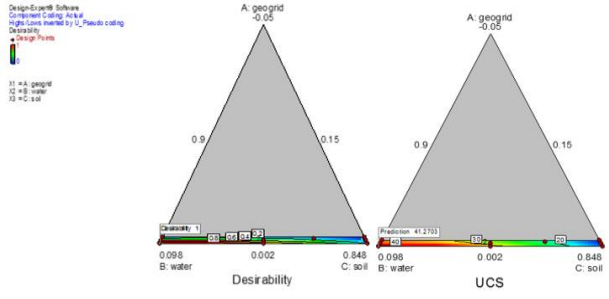

Fig. 19: Contour Plots for the Optimal Solution

4.6.5 3D Surface Plots

3D surface plot is the presentation of the factor levels' relationship with the response functions and for the desirability function shown in Fig. 20 showing an optimal response of 41.270 kN/m^2 and a desirability score of 1 which indicated excellent performance (Goos et al. 2007) [70].

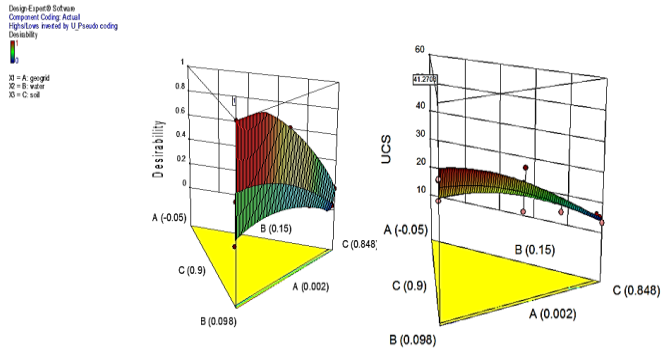

Fig. 20: 3D Plot for the Optimal Solution

4.7. Post Analysis and Model Simulation

The post-analysis result presents the confirmation report at the confidence interval of 95 %, the descriptive statistical computation of the EVD model predicted results, and with the imposition of the sum to one constraint [29-30].

4.7.1 Point Prediction

Point Prediction uses the models fit during analysis and the factor settings specified on the factors tool to compute the point predictions and interval estimates. The predicted values are updated as the levels are changed. Prediction intervals (PI) are found under the confirmation node presented in Table 22 below.

4.7.2 Coefficients Table

The coefficient table shows the factor level combination optimization coefficients of the soil-geogrid blend. This is a table containing one row for each response. If one or more responses have been analyzed, there will be a column for every term from all models. Each column contains the coefficient estimate for the coded model term and the p-value for that coefficient [71]. The quadratic and linear models were adapted simultaneously for the mixture optimization computation. p-values less than 0.01 are very significant and color-coded red; p-values less than 0.05 but greater than 0.01 are significant and color-coded green; p-values less than 0.10 but greater than 0.05 are marginally significant and color-coded blue; p-values greater than or equal to 0.10 are considered insignificant and color-coded black. The coefficient table is presented in Table 23 [29-30].

4.8. EVD Model Simulation

The model simulation stage is the final phase of the model validation process whereby a real-life situation is replicated through what we have modeled to guide contractors, designers, and operators on how the developed EVD model will perform. Furthermore, the essence of model simulation is to show that the validation achieved during statistical inference and diagnostics can be achieved in real-life applicability or situation. Student's t-test and analysis of variance (ANOVA) statistical methods were further deployed to determine if there is a significant difference between the actual experimental values and the generated simulated EVD model results. The computations were carried out by substitution of the developed model coefficients to the factor levels for the mixture design formulation; the computed simulated EVD model results and the actual laboratory results are presented in the plotted graph in Fig. 21.

Table 22: Point Prediction

Response	Predicted Mean	Predicted Median[1]	Observed	Std Dev	SE Mean	CI for 95% CI low	Mean 95% CI high	99% of 95% TI low	Population 95% TI high
UCS[2]	41.2703	41.0699	-	5.74482	N/A	28.2109	56.8211	7.92995	100.023

Table 23: Coefficient Table

Response	A	B	C	AB	AC	BC
UCS	621.935	64.085	11.82484	-663.296	6315.46	3.10192
p =	0.0093	0.0093	0.0093	0.6913	0.7033	0.1973
Legend		P <.01	.01<= P <.05	0.5<= p <.10	p >=.10	

The results of the statistical computation utilized to compare the two sets of means at the confidence interval of 95% are presented in Tables 24-25. From the student t-test computation results, P(T<=t) two-tail of 0.842281, t-Stat of 0.204805, t Critical two-tail of 2.262157 and Pearson correlation score of 79.5% while ANOVA computation results produced, P-value of 0.8412, F critical of 4.413873 and F value of 0.04132 which indicates that there is no significant difference between the actual and EVD model results because obtained p-value or P(T<=t) two-tail were higher than the critical value (0.05); this shows robust performance for the developed EVD model [72-73].

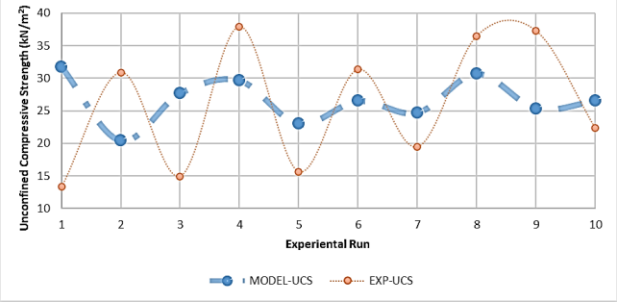

Fig. 21: Simulated EVD Model Results

Table 24: t-Test: Paired Two Sample Means

	MODEL-UCS	EXP-UCS
Mean	26.64599	25.97127
Variance	12.32933	97.85609
Observations	10	10
Pearson Correlation	0.795	
df	9	
t Stat	0.204805	
P(T<=t) one-tail	0.421141	
t Critical one-tail	1.833113	
P(T<=t) two-tail	0.842281	
t Critical two-tail	2.262157	

Table 25: ANOVA Test Results

Groups	Count	Sum	Average	Variance			
MODEL-UCS	10	266.4599	26.64599	12.3293			
EXP-UCS	10	259.7127	25.97127	97.8561			
ANOVA							
Source of Variation	SS	df	MS	F	P-value	F crit	
Between Groups	2.276209	1	2.276209	0.04132	0.841209	4.413873	
Within Groups	991.6688	18	55.09271				
Total	993.945	19					

5. Conclusion

In this research study, geogrids were utilized for engineering properties and modification of soil properties for civil engineering construction purposes. The research process involved the general engineering characteristics determination of the test soil through experimental and laboratory processes to obtain the test soil's general engineering behavior and classification. The results obtained indicated high swelling potential and plasticity behavior with AASHTO classification of A-7 and unsuitable for engineering work.

The I-optimal design was utilized to explore the constrained factor space for the derivation of the run of experiments and mixture proportions formulation at the edges, center, interior, and vertex of the simplex. The mixture of experiment components is constrained by imposed restrictions on the sign of inequalities at the upper and lower region of the factor space to a subregion of the equilateral triangle formed as a result of three-component mixture simplex through the q-vertices with regular sides of (q-1) dimension where q is the total number of mixture ingredients. I-optimality and D-optimality of 0.39093 and 1747.474, respectively, were obtained with a G-efficiency of 64.8%.

The responses were derived from the experimental runs were utilized for the statistical fit test, analysis of variance influence and diagnostic test computation using Design expert and Minitab 18 statistical software which provides an analytical toolbox for the simulation and analysis of mixture experiments for test soil stabilization using geogrids; incorporated in the toolbox are statistical tools and techniques like fit summary, analysis of variance (ANOVA), model equations formulation with coefficients estimation, diagnostic plots utilizing externally studentized residuals for regression model assumptions validation, Box-cox for power transformation, influence plots expressing the cook's distance and leverages vs. Run evaluation, trace plots using cox plot and contour plots.

The numerical and graphical optimization process which locates the factor levels combinations which satisfy the criteria placed on the mixture components and the corresponding response parameters based on the model fitness evaluation through statistical analysis and equation simulation using desirability function was further conducted. A desirability score of 1 was calculated as the optimal solution with the optimal combination ratio of 0.002:0.0.98:0.9 for geogrid, water, and soil, respectively; and an optimal response of 41.270kN/m2 for UCS property.

The results obtained from this research study on geotextile application for expansive soil mechanical properties improvement indicated an improvement in the soil property at 0.2% by volume of geogrid, the generated strength value was greater than the minimum value specified by the American Association of State Highway and Transport Officials (AASHTO) for the mechanical properties of soil.

Finally, the developed EVD model was simulated using the generated model coefficients and compared with the corresponding experimental results using ANOVA and Student's t-test. However, the statistical results showed that there is no significant difference between the compared groups with a p-value of 0.841209 and P(T<=t) two-tail 0.842281 which is greater than a critical value (α).

Conflict of Interests Declaration

The authors declare no conflicting interests in this research paper.

REFERENCES

[1] Salahudeen, A. B., Eberemu O. A., and Osinubi, K. J., Assessment of cement kiln dust-treated expansive soil for the construction of flexible pavements. Geotechnical and Geological Engineering, Springer, Vol. 32, 2014, No. 4, PP. 923-931.

[2] I. Al-Qadi, S. Dessouky, J. Kwon, and E. Tutumluer,"Geogrid in flexible pavements: validated mechanism," Transportation Research Record: Journal of the Transportation Research Board,

no. 2045, pp. 102-109, 2008.

[3] Buonsanti, M.; Leonardi, G.; Scopelliti, F. Theoretical and computational analysis of airport flexible pavements reinforced with geogrids. In 7th RILEM International Conference on Cracking in Pavements; Springer: Dordrecht, the Netherlands; Berlin/Heidelberg, Germany, 2012; pp. 1219–1227.

[4] A. Demir, M. Laman, A. Yildiz, and M. Ornek, "Large scale field tests on geogrid-reinforced granular fill underlain by clay soil," Geotextiles and Geomembranes, vol. 42, pp. 1–15, 2012

[5] B. Indraratna, N. T. Ngo, and C. Rujikiatkamjorn, "Behavior of geogrid-reinforced ballast under various levels of fouling," Geotextiles and Geomembranes, vol. 29, no. 3, pp. 313–322, 2011

[6] H. A. Alawaji, "Settlement and bearing capacity of geogrid reinforced sand over collapsible soil," Geotextiles and Geomembranes, vol. 19, no. 2, pp. 75–88, 2001.

[7] Mehrjardi GT, Ghanbari A and Mehdizadeh H. Experimental study on the behaviour of geogrid-reinforced slopes with respect to aggregate size. Geotextiles Geomembranes 2016; 44(6): 862–871.

[8] Bao CG, Wang MY and Ding JH. Mechanism of soil reinforced with geogrid. Journal of Yangtze River Scientific Research Institute 2013; 30(1): 34–41.

[9] Jia-Quan Wang, Liang-Jie Xu, Zhi-Nan Lin, Yi Tang. (2020). Study on creep characteristics of geogrids considered sand-geosynthetics interaction under different loading levels. Journal of Engineered Fibers and Fabrics Volume 15: 1–12. DOI: 10.1177/1558925020958520.

[10] K. Onyelowe, G. Alaneme, D. Bui Van, M. Nguyen Van, C. Ezugwu, T. Amhadi, F. Sosa, F. Orji, and B. Ugorji, Generalized Review on EVD and Constraints Simplex Method of Materials Properties Optimization for Civil Engineering, Civil Engineering Journal (5) (2019) 729-749, http://dx.doi.org/10.28991/cej-2019-03091283

[11] K.C. Onyelowe, G. Alaneme, C. Igboayaka, F. Orji, H. Ugwuanyi, D. Bui Van, M. Nguyen Van, Scheffe optimization of swelling California bearing ratio, compressive strength, and durability potentials of quarry dust stabilized soft clay soil, Mater. Sci. Energy Technol. 2 (1) (2019) 67 77. https://doi.org/10.1016/j.mset.2018.10.005.

[12] Liu, Y., Su, Y., Namdar, A., et al., Utilization of cementitious materials from residual rice husk ash and lime in stabilization of expansive soil. Advances in Civil Engineering, Vol. 2019, and article ID: 5205276. https://doi.org/1155/2019/5205276

[13] Irving Cruz-Matíasa, Dolors Ayalab, Daniel Hillerc, Sebastian Gutschd, Margit Zachariasd, Sònia Estradée, f, Francesca Peiróe, Sphericity and roundness computation for particles using the extreme vertices model, Journal of Computational Science 30 (2019) 28–40, https://doi.org/10.1016/j.jocs.2018.11.005 1877-7503

[14] Faula Arina, Aji Hamim Wigena, I Made Sumertajaya2, Utami Syafitri, Split Plot Mixture Process Variable Experiment on Steel Slag Concrete, IOP Conf. Series: Earth and Environmental Science 187 (2018) 012049, doi :10.1088/1755-1315/187/1/012049.

[15] R. A. McLean and V. L. Anderson (2012) "Extreme Vertices Design of Mixture" University of Tennessee, United States.

[16] Damiri S, Pouretedal HR, Bakhshi O. (2016). 'An extreme vertices mixture design approach to the optimization of methylal production process using p-toluenesulfonic acid as catalyst'. Chem Eng Res Des 2016;112:155–62

[17] J. A. Cornell, Experiments with Mixtures: Designs, Models, and the Analysis of Mixture Data, John Wiley & Sons, New York, NY, USA, 3rd edition, 2011.

[18] J. A. Cornell, Experiments with Mixtures: Designs, Models, and the Analysis of Mixture Data, John Wiley & Sons, New York, NY, USA, 3rd edition, 2011.

[19] H. Scheffé, Experiments with mixtures. Journal of the Royal Statistical Society Series B. 20, (1958), 344-360.

[20] D. Jian-Tong, Y. Pei-Yu, L. Shu-Lin, Z. Jin-Quan, Extreme vertices design of concrete with combined mineral admixtures. Cement and Concrete Research, 29(6) (1999) 957-960. http://dx.doi.org/10.1016/S0008-8846(99)00069-1

[21] Calvarano, L.S.; Palamara, R.; Leonardi, G.; Moraci, N. Unpaved Road Reinforced with Geosynthetics. Procedia Eng. 2016, 158, 296–301.

[22] British Standard (BS) 1377 (1990) Method of testing soils for civil engineering purpose. British Standards Institution, London

[23] British Standard (BS) 1924 (1990) Method of testing for stabilized soils. British Standard Institution, London

[24] Aslam, F., Farooq, F., Amin, M. N., et al., Application of gene expression programming for estimating compressive strength of high-strength concrete. Advances in Civil Engineering, Vol. 2020, article ID: 8850535. https://doi.org/10.1155/2020/8850535

[25] W. Wangkananon, C. Phuaksaman, T. Koobkokkruad, S. Natakankitkul, An extreme vertices mixture design approach to optimization of tyrosinase inhibition effects. Engineering Journal, 22 (1) (2018) http://dx.doi.org/10.4186/ej.2018.22.1.175

[26] Aji Hamim Wigena, I Made Sumertajaya and Utami Syafitri, Constrained Experimental Regions on Ground Granulated Blast Furnace Slag Concrete, Applied Mathematical Sciences, Vol. 12, 2018, no. 26, 1251 1258. https://doi.org/10.12988/ams.2018.89128

[27] Guimarães MGA, de Mattos VD, de Carvalho U, et al. Degradation of polypropylene woven geotextile: tensile creep and weathering. Geosynth Int 2017; 24(2): 213–223

[28] Wang JQ, Zhou J and Deng YB. Macro-Mesoscopic study of the interface between sand and geogrid[C]//Geotechnical Special Publication No.207, In: GeoShanghai international conference, Shanghai, China, 3–5 June 2010, pp. 361–366.

[29] Design expert 11. Design of experiment software, Stat-Ease Inc., Minneapolis, USA. 2018.

[30] Minitab 18. Minitab statistical software, Minitab Inc., Pennsylvania, USA. 2018.

[31] Kwok CCHCM. Parametric studies of the behaviour of a reinforced embankment. Geotextiles, Geomembranes, and Related Products: steep slopes and walls. Embankments on soft soil. Roads and railroads. Filtration and drainage. Erosion control 1990; 1: 137.

[32] Pinho-Lopes M, Paula AM and Lopes ML. Long-term response and design of two geosynthetics: effect of field installation damage. Geosynth Int 2018; 25(1): 98–117

[33] Zhou J, Chen JF, Xue JF, et al. Micro-mechanism of the interaction between sand and geogrid transverse ribs. Geosynth Int 2012; 19(6): 426–437.

[34] J. Schwartz, S. Merck, R. L. Dohme, Optimization techniques in product formulation. J Soc Cosmet Chem., 32 (1981) 287-301.

[35] Lawson J, Erjavec J (2001). Modern Statistics for Engineering and Quality Improvement.Duxbury, Pacific Grove.

[36] U. Syafitri, B. Sartono, P. Goos, I-optimal design of mixture experiments in the presence of ingredient availability constraints. J. Qual. Technol. 47 (2015) 220–234.

[37] Ding JT, Yan PY, Liu SL, Zhu JQ. (1999). 'Extreme vertices design

of concrete with combined mineral admixtures'. Cem Concr Res 1999; 29(6):957–60, http://dx.doi.org/10.1016/S0008-8846(99)00069-1.

[38] Xue JF, Chen JF, Liu JX, et al. Instability of a geogrid reinforced soil wall on thick soft Shanghai clay with prefabricated vertical drains: a case study. Geotextiles Geomembranes 2014; 42(4): 302–311

[39] Alaneme, G. U., Onyelowe, K. C., Onyia, M. E., Bui Van, D., Mbadike, E. M., Dimonyeka, M. U., Attah, I. C., Ogbonna, C., Iro, U. I., Kumari S., Firoozi A. A., and Oyagbola I. (2020). Modelling Of The Swelling Potential Of Soil Treated With Quicklime-Activated Rice Husk Ash Using Fuzzy Logic, Umudike Journal of Engineering and Technology (UJET); Vol. 6, No. 1, June 2020, pp. 1 – 22; Michael Okpara University of Agriculture, Umudike, Print ISSN: 2536-7404, Electronic ISSN:2545-5257; http://ujetmouau.net; doi: https://doi.org/10.33922/j.ujet_v6i1_1

[40] Standard Specifications for Transportation, Material and Method of Sampling and Testing, 14th Edition, American Association of State Highway and Transportation Official (AASHTO) Washington D.C. 1986

[41] American Standard for Testing Material, Annual Book of Standards Vol. 04.08, American Society for Testing and Materials, Philadelphia. 1992.

[42] Federal Ministry of Works and Housing (1997) General Specification for Roads and Bridges, Volume II, Federal Highway Department, FMWH: Lagos, Nigeria, 317 p.

[43] Bello, A. A., Ige, J. A., and Tajudeen, S. 2007. Geotechnical characterization of lateritic Soils in parts of Ejigbo Local Area, South-western Nigeria. LAUTECH J. Engr. Technol. 4(2): 34 – 38.

[44] Kennedy Chibuzor Onyelowe, Duc Bui Van & Manh Nguyen Van (2018) "Swelling potential, shrinkage and durability of cemented and uncemented lateritic soils treated with CWC base geopolymer", International Journal of Geotechnical Engineering

[45] G. A. Miller, M. Zaman, Field and laboratory evaluation of cement kiln dust as a soil stabilizer. Transp. Res. Rec., 1714 (2000) 25–32.

[46] A. B. Salahudeen, T. S. Ijimdiya, A. O. Eberemu, K. J. Osinubi, Artificial neural networks prediction of compaction characteristics of black cotton soil stabilized with cement kiln dust. J Soft Comput Civ Eng 2(3) (2018) 53–74.

[47] A. B. Salahudeen, O. A. Eberemu, K. J. Osinubi, Assessment of cement kiln dust-treated expansive soil for the construction of flexible pavements. Geotechnical and Geological Engineering, Springer, 32(4) (2014) 923-931.

[48] Alaneme George, U. & Mbadike Elvis, 'Modelling of the mechanical properties of concrete with cement ratio partially replaced by aluminium waste and sawdust ash using artificial neural network', M. SN Appl. Sci. (2019) 1: 1514. https://doi.org/10.1007/s42452-019-1504-2

[49] Provenzano P, Ferlisi S, Musso A. Interpretation of a model footing response through an adaptive neural fuzzy inference system. Comput Geotech 2004;31:251–66.

[50] D. W. Marquardt, R. D. Snee, Test statistics for mixture models, Technometrics, 14 (1974) 533-537.

[51] Stahle L, Wold S. Analysis of variance (ANOVA). ChemometrIntell Lab Syst 1989;6:259–72,http://dx.doi.org/10.1155/2018/9308580.

[52] R. D. Snee, Experiment design for mixture systems with multicomponent constraints. Commun. Stat. Theory Methods, 17 (1979) 149–159.

[53] Akhnazarova, S., &Kafarou, V. (1982). "Experiment optimization in Chemistry and chemical engineering", MIR publishers, Moscon.

[54] A. C. Atkinson, A. N. Donev, R. D. Tobias, Optimal experimental design with SAS; Oxford University Press: Oxford, UK, 2007.

[55] McLean, R. A. and Anderson, V. L. (1966). 'Extreme Vertices Design of Mixture Experiments. Technometrics', 8(3) 447-454.

[56] Kumar RG, Sanghvi I. Optimization techniques: an overview for formulation development. Asian J Pharm Res 2015;5:217-21.

[57] R. Shobha, R. Hiremath, K. Vanaja, Optimization techniques in pharmaceutical formulation and processing. Textbook of Industrial Pharmacy. Drug Delivery Systems, Cosmetic and Herbal Drug Technology, (2016) 158-68.

[58] S. Bolton, Optimization techniques in pharmaceutical statistics. Practical and clinical Applications. 3rded. New York: Marcel Dekker; 1997.

[59] J. J. Borkowski, Using genetic algorithm to generate small exact response surface designs. J. Probab. Stat. Sci. 1 (2003) 65–88.

[60] Brereton R. G., Chemometrics: Data Analysis for the Laboratory and Chemical Plant, John Wiley & Sons, West Sussex, UK, 2003.

[61] W. F. Smith, Experimental design for formulation, The American Statistical Association and the Society for Industrial and Applied Mathematics: Philadelphia, PA, USA, 2005

[62] J. W. Gorman, Fitting equations to mixture data with restraints on compositions. J. Quality Tech., 2 (1970) 186-194.

[63] G. E. P. Box, N. R. Draper, A basis for the selection of a response surface design. J. Am. Stat. Assoc. 54 (1959) 622–654

[64] Piepel GF (1988). "Programs for Generating Extreme Vertices and Centroids of Linearly Constrained Experimental Regions." Journal of Quality Technology, 20, 125–139.

[65] Fedorov, V.V. Theory of Optimal Experiments; Academic Press: New York, NY, USA, 1972.

[66] R. H. Hardin, N. J. A. Sloane, A new approach to construction of optimal designs. J. Stat. Plan. Inference 37 (1993) 339–369.

[67] Sahni NS, Piepel GF, Naes T (2009). "Product and Process improvement Using Mixture- Process Variable Methods and Robust Optimization Techniques." Journal of Quality Technology, 41, 181–197.

[68] A. Ozol-Godfrey, C. M. Anderson-Cook, D. C. Montgomery, Fraction of design space plots for examining model robustness. J. Qual. Technol. 37 (2005) 223–235.

[69] Myers RH, Montgomery DC (2002). 'Response Surface Methodology: Process and Product Optimization Using Designed Experiments'. 2nd edition. John Wiley & Sons, New York.

[70] Goos P, Donev AN (2007). "Tailor-Made Split-Plot Designs for Mixture and Process Variables." Journal of Quality Technology, 39, 326–339.

[71] Bates D, Mächler M, Bolker B, Walker S (2015). "Fitting Linear Mixed-Effects Models Using lme4." Journal of Statistical Software, 67(1), 1–48. doi:10.18637/jss.v067.i01.

[72] Alaneme, G.U., Ezeokpube, G.C. & Mbadike, E.M. Failure Analysis of a Partially Collapsed Building using Analytical Hierarchical Process. J Fail. Anal. And Preven. (2020). https://doi.org/10.1007/s11668-020-01040-3

[73] Coetzer, R.; Haines, L.M. The construction of D- and I-optimal designs for mixture experiments with linear constraints on the components. Chemom. Intell. Lab. Syst. 2017, 171, 11